Magnesium–lithium alloys with TiB and Sr additions

Mariusz Król[1] 🆔

Abstract

The ultralight hypoeutectic α-phase Mg–4.5Li–1.5Al alloy and hypereutectic β-phase Mg–12Li–1.5Al alloy in as-cast state were fabricated and subjected to modification by 0.2 mass% TiB and 0.2 mass% Sr grain modifiers. The crystallisation sequence of Mg–Li–Al alloys has been investigated in detail by using thermal-derivative analysis and microstructural observations. The presented work includes the effects of grain refiners on grain size and microstructure and thermal events registered during crystallisation of ultralight Mg–Li–Al alloys by recording and analysis of the temperature vs time, i.e. as T_N, T_α, T_β, $T_{\eta(LiAl)}$ and T_{SOL}. Microstructure and phase observation has been done by light microscope, X-ray diffraction and energy dispersive X-ray spectroscopy. The changes of characteristic temperature points for phase transformation are studied in detail. Due to the addition of 0.2 mass% TiB and 0.2 mass% Sr, the grain structure of the alloy was refined, and mechanical properties were improved. When a TiB and Sr added simultaneously, the average grain size of the analysed alloys strongly decreases. When the TiB or Sr content was severally added, a low effect of improvements of mechanical properties was observed. With the TiB and Sr content, the liquidus and solidus decrease gradually.

Keywords Mg–Li · Grain refiners · Thermal-derivative analysis · Mechanical properties

Introduction

Looking for new materials that meet the requirements of modern constructions, minimising mass while maintaining high properties and even increasing durability lead to the development and testing of magnesium alloys belonging to the group of light alloys [1–3].

This material has been used in various industries for many decades, showing a growing trend and increasing its popularity, from the automotive or aerospace industries, through electronic, sports, weapons to the space industry. Magnesium alloys give the potential for mass and associated energy savings in both the automotive and aerospace applications as all possess the highest strength-to-mass ratio to basic structural alloys. Despite the expensive cost, this potential advantage has led to a recent rise in interest on the cast and wrought magnesium components [2–4].

The unfavourable tendency of using only standard Mg alloys has led to limiting the development of more demanding and complex varieties. Discontinued due to insufficient footing properties in the past, after their improvement they are experiencing resurgence and placing today the third place among the numerous commonly used materials in the automotive industry [5–7].

The main focus is on the modification of magnesium using alloying elements and the development of the manufacturing process, which is high-pressure casting, characterised by ever better production efficiency and a beneficial effect on the properties of the material [8].

One of the tested magnesium alloys is those with the addition of lithium, forming ultralight alloys with high stiffness and good plastic deformability. Despite the features mentioned, their use is still limited due to insufficient strength and corrosion resistance. It is worth noting that research and hopes about Mg–Li alloys, their modifications and finding of the gold in the case of alloy additives are being carried out all over the world [9, 10].

To magnesium alloys, grain refinement is essential as an excellent grain size generally leads to developed mechanical features and a more uniform concentration of

✉ Mariusz Król
  mariusz.krol@polsl.pl

[1] Institute of Engineering Materials and Biomaterials, Faculty of Mechanical Engineering, Silesian University of Technology, Konarskiego 18a St., 44-100 Gliwice, Poland

secondary phases and solute elements on a fine scale which results in greater machinability [11–14].

It is well identified that Al–5Ti–B master alloy is an efficient grain refiner in aluminium alloys; however, nowadays researchers start to pay increased attention to the influences of Al–TiB additions on the grain size of Mg-based alloys.

This work focused on analysis of the crystallisation sequence of the ternary hypoeutectic single-α-phase Mg–4.5Li–1.5Al and hypereutectic β-phase Mg–12Li–1.5Al alloys detail by first derivative, mainly, on the analysis of critical temperatures and transitions during crystallisation. The microstructure observation, computer-aided cooling curve analysis and X-ray diffraction (XRD) were applied for phase identification to define the influence of applied grain modifiers.

Experimental

The as-cast magnesium–lithium–aluminium alloys: Mg–4.5Li–1.5Al and Mg–12Li–1.5Al, were used in this study. The analysed magnesium alloys were selected based on a binary system of Mg–Li diagram (Fig. 1) characterised as single α- and β-phase structure. Commercial pure magnesium (min. 99.5%), lithium (99.9%) and aluminium (99.98%) and TiB and Sr were added into mild steel crucible placed in induction heater VSG 02 from the Balzers Company. For the production of alloys, high-purity Mg ingots were smelted in a steel crucible in argon-protective atmosphere at 700–720 °C at a pressure of 650 torr, to reduce the evaporation of elements. The alloys were cast gravitationally into the cold mould of graphite in rod-

shaped ingots with dimensions ø20 × 100 mm. The analysis of chemical composition of elements in analysed ultralight Mg–Li alloys was specified by the ICP-OES method. The measurements results of the analyses are listed in Table 1. The chemical composition of used grain refinements is given in Table 2. The master alloys were provided by Institute of Non-Ferrous Metals, Light Metals Division in Skawina, Poland.

Measurements of Al, Li, B, Si, Ti, V, Fe, Sr and Ca contents in the obtained solutions were made using the inductively coupled optical emission spectrometer with inductively coupled plasma (ICP-OES) Optima 5300 V, manufactured by PerkinElmer. The samples were taken in a mixture of nitric (V) and hydrochloric acids with the addition of hydrofluoric acid.

The thermal-derivative analysis (TDA) of melting and solidification series was carried out using the Universal Metallurgical Simulator and Analyser (UMSA). Specimens for thermal treatment were cut from the same position of the cast ingots and processed into cylinders of 18 mm in diameter and 20 mm in length. The data for TDA were collected using a high-speed National Instruments data acquisition system linked to a personal computer. The signal in the form of heating and cooling curves was measured during the melting and solidification cycles. The temperature versus time and first derivative versus temperature were calculated and plotted. One shielded K-type thermocouple was immersed in the melt from the top. The average cooling rate between liquidus and solidus temperature was approx. 0.6 °C s^{-1}. The Fityk software was used for the analysis of obtained results. In order to determine a crystallisation process of analysed materials, the cooling curves and corresponding first derivative were plotted. The baseline was determined based on the Newtonian method. The baseline has been predicted by sixth polynomial fitting $(dT/dt)_{BL} = a_0 + a_1T + a_2T^2 + a_3T^3 + a_4T^4 + a_5T^5 + a_6T^6$. The sixth-order polynomial yields a correlation coefficient higher than 0.98. Thermal-derivative analysis was made at least three times per alloy. The presented values in tables are average values.

A small cross section was cut from the same part of the cast alloy sample for metallographic observations. The microstructure and morphology of the analysed materials were observed using Leica microscope with Q-WinTM image analyser software. The linear intercept method was applicable for average grain size measurements. To reveal a microstructure of analysed alloys, etchant composed of 1 mL HNO$_3$, 24 mL water and 75 mL ethylene glycol was used. The etchant time was approx. 10 s.

The alloy was subjected to X-ray diffraction (XRD) using a X'Pert diffractometer to analyse the alloy sample composition and phases. For X-ray diffraction analysis, a
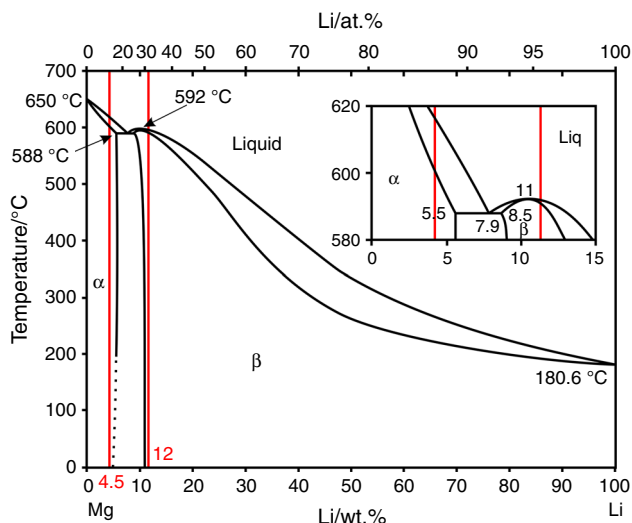

Fig. 1 Binary system of analysed Mg–Li alloys [15]

Table 1 Analysed chemical composition of the as-cast Mg–Li–Al alloys

An alloy	Li	Al	Si	B	Ti	Sr	V	Ca	Fe	Mg
Mg–4.5Li–1.5Al	4.64	1.86	–	–	–	–	–	–	–	Balance
Mg–4.5Li–1.5Al + 0.2TiB	4.66	1.80	0.0052	0.0019	0.0069	–	–	–	0.0019	Balance
Mg–4.5Li–1.5Al + 0.2Sr	4.63	1.80	0.030	–	–	0.019	–	0.018	–	Balance
Mg–4.5Li–1.5Al + 0.2 TiB + 0.2Sr	4.63	1.85	0.041	0.0012	0.0042	0.021	< 0.001	0.0023	< 0.001	Balance
Mg–12Li–1.5Al	12.00	1.80	–	–	–	–	–	–	–	Balance
Mg–12Li–1.5Al + 0.2 TiB	12.00	1.75	0.040	0.0021	0.0091	–	< 0.001	–	0.0012	Balance
Mg–12Li–1.5Al + 0.2Sr	12.00	1.78	0.027	–	–	0.025	–	0.0053	–	Balance
Mg–12Li–1.5Al + 0.2 TiB + 0.2Sr	12.00	1.77	0.028	0.0028	0.013	0.020	< 0.001	0.0067	0.0017	Balance

Table 2 Chemical composition of TiB and Sr master alloys used as grain refinements

An alloy	Ti	B	Fe	Si	V	Sr	Ca	Al
TiBor	4.9	0.95	0.17	0.06	0.09	–	–	Balance
AlSr	–	–	0.13	0.08	–	10.7	< 0.10	Balance

Co target, a scan rate of 0.03 step/s and a scan range of 2θ of 30–110° were used.

The Zwick ZHR 4150 TK hardness tester in the HRF scale was used for hardness measurements.

Results and discussion

Figure 2 displays the X-ray diffraction patterns of analysed Mg–Li–Al alloys. The alloys with 4.5 mass% lithium consisted of the single α-Mg phase (solid solution of lithium in magnesium). The XRD profile of 12 mass% Li alloy demonstrates that the analysed alloy consists of single-phase–β-Li phase (a solid solution of magnesium in lithium). The presented XRD results are faithful with analysis of microstructure using a LOM (Fig. 3). The XRD analysis revealed that aluminium does not create any new phases, which indicates that aluminium is present in a solid solution. Moreover, addition of TiB and Sr does not affect the appearance of new phases.

Figures 3 and 4 show the microstructure of Mg–4.5Li–1.5Al and Mg–12Li–1.5Al in as-cast alloys and after treatment by TiB and Sr. When TiB and Sr were added to the alloy, the α-magnesium and β-lithium grains in the alloy were refined, and the grain morphology becomes with a granular shape.

In summary, it can be concluded that the microstructure is formed of α- and β-phases which is consistent with the
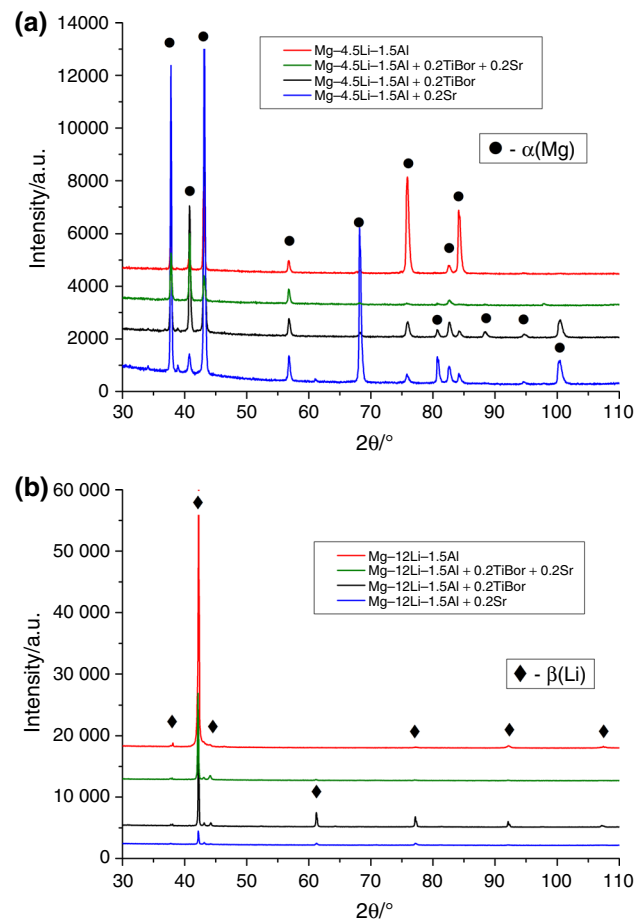
Fig. 2 XRD profiles of: **a** Mg–4.5Li–1.5Al and **b** Mg–12Li–1.5Al treated by TiB and Sr as grain modifiers

Mg–Li phase diagram [16, 17]. XRD analysis confirms the occurrence of main phases in analysed materials.

Measurements of the average grain size of analysed alloys determined by line intersect method exhibit that the modification level is different for every analysed alloys (Figs. 3, 4). When the TiB is applied, a notable decrease in

Fig. 3 Microstructures of Mg–4.5Li–1.5Al in as-cast state (**a**), treated by TiB (**b**) and Sr (**c**) and TiB + Sr (**d**)
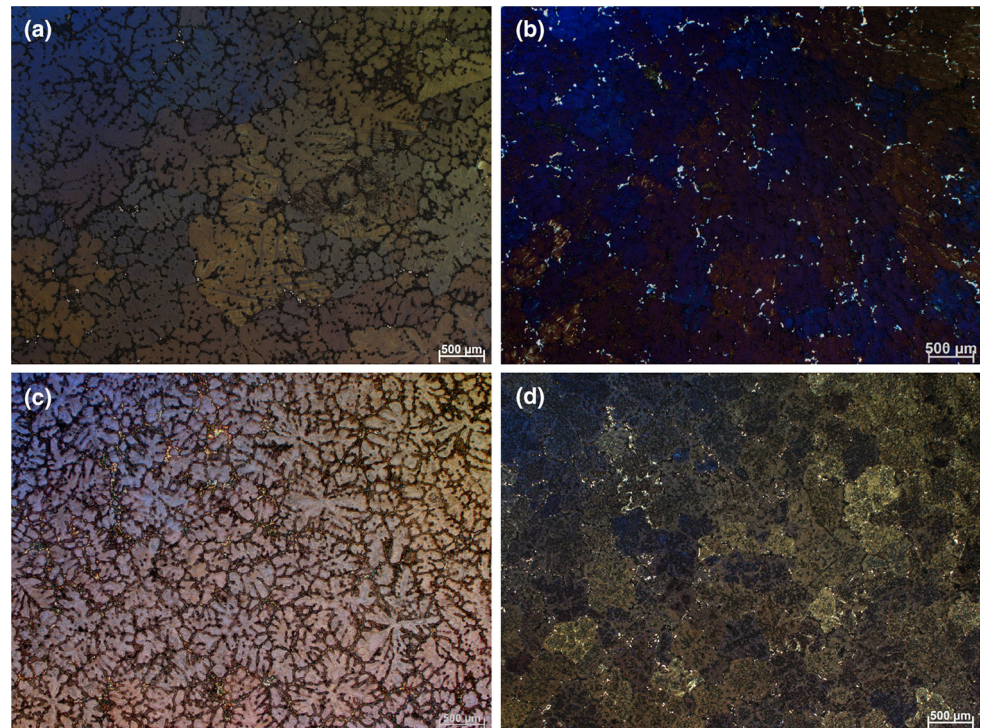
average grain size is observed. The grain size of Mg–4.5Li–1.5Al alloy decreased from 996 to 523 μm with 0.2 mass% TiB (Fig. 5). The measurements exhibit that the application of Sr reduces the average grain size of Mg–4.5Li–1.5Al alloy to 630 μm, while the simultaneous application of TiB and Sr causes a decrease in average grain size to 439 μm.

Measurements of average grain size of Mg–12Li–1.5Al alloy present that application of TiB as a grain refinement causes the reduction in average grain size from 628 to 385 μm. The measurements exhibit that the application of Sr has influence on a decrease of average grain size to 483 μm, while the addition of TiB and Sr simultaneously decreased the average grain size to 394 μm. Moreover, it can be noticed that with an increment of Li content from 4.5 to 12 mass%, a decrement of average grain size can be observed.

Measurements of hardness according to the Rockwell method in F scale of alloys after thermal treatment display that the grain refinements affect the average hardness of analysed alloys (Fig. 6). When 0.2 mass% of TiB is added, the significant increment of average hardness in the Mg–4.5Li–1.5Al alloy from 34 to 40 HRF can be observed. The measurements indicate that the application of Sr slightly reduces the average hardness of Mg–4.5Li–1.5Al alloy to 31 HRF; meanwhile, the application of TiB and Sr simultaneously causes increases in average hardness to 44 HRF. The same situation is observed when the 0.2 mass% of TiB is added to analysed Mg–12Li–1.5Al alloy; i.e.

significant increment of average hardness from 70 to 79 HRF can be observed. The results indicate that the application of Sr slightly decreases the average hardness of Mg–12Li–1.5Al cast alloy to 75 HRF, and similarly, the application of TiB and Sr simultaneously causes a decrement in average hardness to 73 HRF. Moreover, it can be noticed that with an increment of Li content from 4.5 to 12 mass%, an increment of the average hardness of analysed alloys can be observed.

The solidification sequence of as-cast Mg–4.5Li–1.5Al alloy (Fig. 7a) and after addition of 0.2 mass% TiB (Fig. 7b) and 0.2 mass% Sr (Fig. 7c) and 0.2 mass% TiB and Sr (Fig. 7d) has been analysed by computer-aided cooling curve method (Table 2). Figure 7a exhibits three lines, i.e. cooling curve, crystallisation curve and baseline that were basis for establishing critical events during crystallisation process. Analysed Mg–Li–Al alloy with 4.5 mass% Li and four well-defined reactions are recognised, i.e. at 606.06 °C [1—T_N—nucleation temperature (liquidus temperature)], 600.53 °C (2—$T_{\alpha,G}$—α-Mg growth temperature), nucleation of η(LiAl) phase at 545.38 °C and 524.17 °C (T_{SOL}—solidus temperature). The TDA analysis revealed that the addition of TiB and Sr does not affect the appearance of new reactions. Results from the thermal-derivative analysis (Table 3) present that the application of 0.2 mass% TiB and Sr causes changes in the nucleation temperature, i.e. from 606.06 to 602.51 °C, and decrement in solidus temperature from 524.17 to 491.23 °C of analysed alloys. Addition of grain

Fig. 4 Microstructures of Mg–12Li–1.5Al in as-cast state (**a**) and treated by TiB (**b**) and Sr (**c**) and TiB + Sr (**d**)

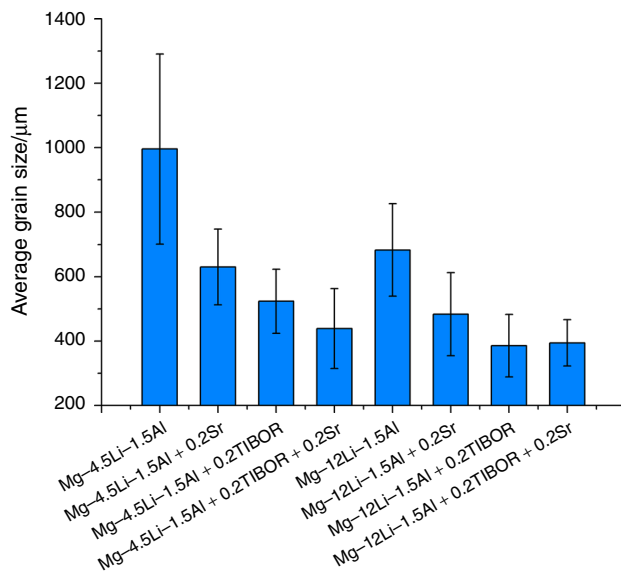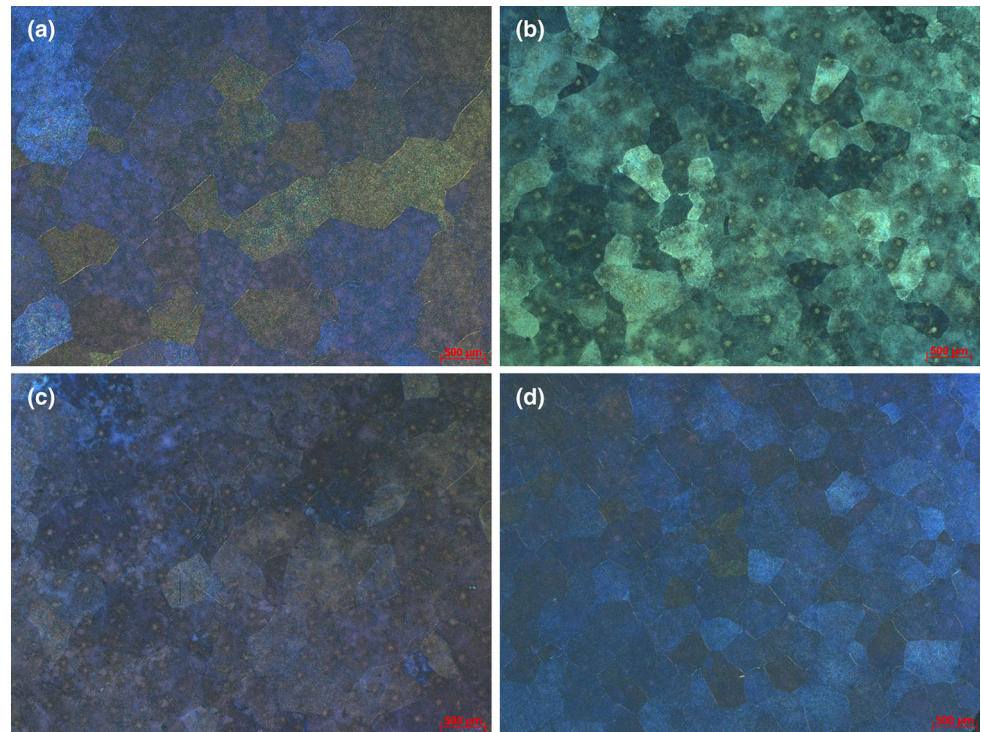Fig. 5 Variation of grain size of as-cast alloys with the addition of TiB and Sr grain modifiers

Fig. 6 Variation of hardness of as-cast alloys with the addition of TiB and Sr grain modifiers

refinements causes slight decrement in $T_{\alpha,\mathrm{G}}$—α-Mg growth temperature from 600.53 to 597.25 when TiB is added, to 599.09 when Sr is added and 598.14 when TiB and Sr are added simultaneously. The solidification period at the cooling rate of 0.6 °C s^{-1}, in Mg–4.5Li–1.5Al and Mg–12Li–1.5Al, reached $\Delta t = 138$ and 104.4 s, respectively.

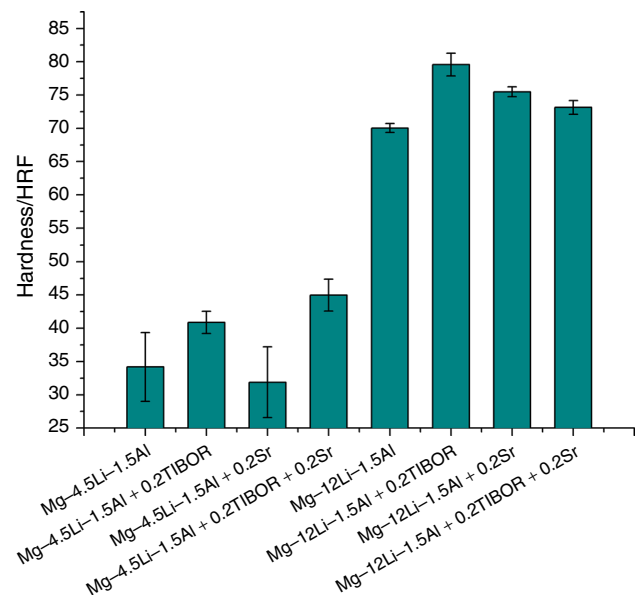When TiB and Sr are added to the analysed alloys, occurrence of new exothermic peak (designated as point 4 in Fig. 7a–d) presumably comes from the crystallisation of
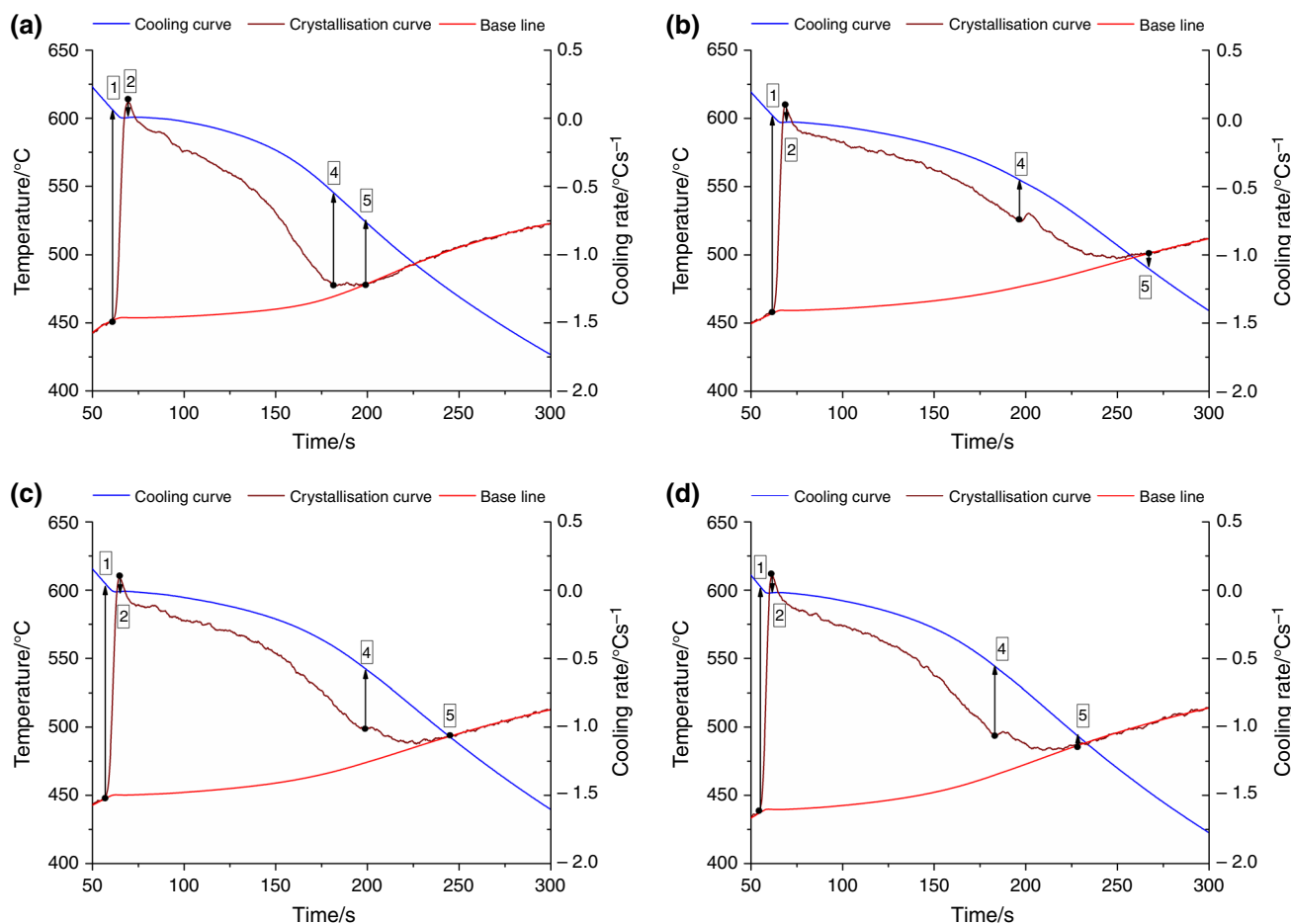
Fig. 7 Thermal-derivative analysis results of: **a** Mg–4.5Li–1.5Al, **b** Mg–4.5Li–1.5Al + 0.2TiB, **c** Mg–4.5Li–1.5Al + 0.2Sr, **d** Mg–4.5Li–1.5Al + 0.2TiB + 0.2Sr

Table 3 Solidification characteristics of modified Mg–4.5Li–1.5Al alloy

Reaction/°C		Mg–4.5Li–1.5Al	Mg–4.5Li–1.5Al + 0.2TiB	Mg–4.5Li–1.5Al + 0.2Sr	Mg–4.5Li–1.5Al + 0.2TiB + 0.2Sr
1	T_N—nucleation temperature (liquidus temperature)	606.06	607.90	605.26	602.51
2	$T_{\alpha,G}$—α-Mg growth temperature	600.53	597.25	599.09	598.14
3	$T_{\beta,G}$—β-Li growth temperature	–	–	–	–
4	$T_{\eta(LiAl)}$-nucleation of η(LiAl) phase	545.38	554.49	542.46	543.55
5	T_{SOL}—solidus temperature	524.17	492.31	493.24	491.23

(–) reaction not observed

metastable intermetallic phase η(LiAl) with B2 structure [16–18]. 4—$T_{\eta(LiAl)}$—nucleation of η(LiAl) phase is observed at 554.49 °C (Mg–4.5Li–1.5Al + TiB), 542.46 °C (Mg–4.5Li–1.5Al + Sr) and 543.55 °C (Mg–4.5Li–1.5Al + 0.2TiB + 0.2Sr).

The crystallisation sequence of analysed Mg–4.5Li–1.5Al alloys, based on first derivative analysis,

microstructure examination and research of phase diagrams [16, 17] may be described as:

1. $L \rightarrow \alpha(Mg)$
2. α-Mg growth temperature
3. $\alpha(Mg) \rightarrow \alpha(Mg) + \eta(LiAl)$

In the first stage, the hcc of α(Mg) begins to crystallise, until the liquid composition leads to the β-Li growth temperature. After passing that temperature, transformation in solid state occurs (solvus line in Mg–Li binary system) resulting in appearance of α(Mg) and η(LiAl) intermetallic compound with B2 structure. Crystallisation process finished with solidus temperature.

Additions of grain refinements to the Mg–12Li–1.5Al alloy result in slight reduction in nucleation temperature to 581.16 °C (with TiB + Sr) but highly decrease a solidus temperature from 553.48 to 518.07 °C concerning the unmodified alloy. Based on first derivative analysis (Fig. 8 and Table 4), it was discovered that application of TiB and Sr simultaneously results in reduction in $T_{\beta,G}$–β-Li growth temperature from 580.08 to 573.99 °C.

It is summarised that thermal-derivative analysis did not detect any additional reaction such as precipitation of

Mg$_2$Sr, with high melting temperature 680 °C as presented in works [16, 17]. This situation can be caused that the level of Mg$_2$Sr intermetallic phase is very low below the detection level of the method.

The transformation sequences during crystallisation of Mg–12Li–1.5Al alloys, based on first derivative, microstructure analysis and study of phase diagrams [16, 17] may be described as follows:

1. $L \rightarrow \beta(Li)$
2. β-Li growth temperature
3. $\beta(Li) \rightarrow \beta(Li) + \eta(LiAl)$

In the first stage, the β(Li) is formed, until the liquid composition reaches the β-Li growth temperature. Then, transformation in solid state happens causing formation of β(Li) phase and η(LiAl) intermetallic phase with B2
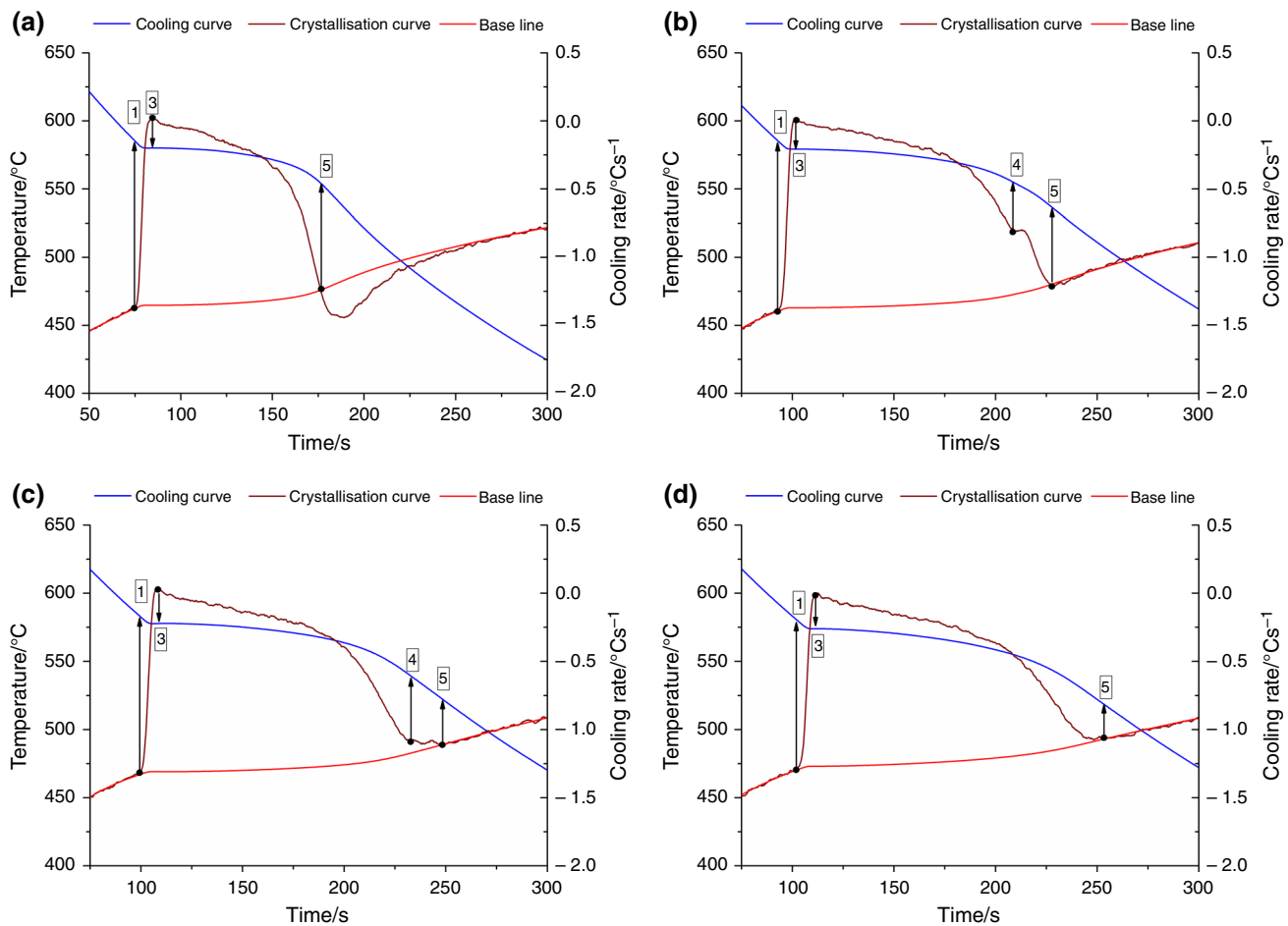

Fig. 8 Thermal analysis results of: **a** Mg–12Li–1.5Al, **b** Mg–12Li–1.5Al + 0.2TiB, **c** Mg–12Li–1.5Al + 0.2Sr, **d** Mg–12Li–1.5Al + 0.2TiB + 0.2Sr

Table 4 Solidification characteristics of modified Mg–12Li–1.5Al alloy

Reaction/°C		Mg–12Li–1.5Al	Mg–12Li–1.5Al + 0.2TiB	Mg–12Li–1.5Al + 0.2Sr	Mg–12Li–1.5Al + 0.2TiB + 0.2Sr
1	T_N—nucleation temperature (liquidus temperature)	585.84	585.83	583.00	581.16
2	$T_{\alpha,G}$—α-Mg growth temperature	–	–	–	–
3	$T_{\beta,G}$—β-Li growth temperature	580.08	579.26	577.8	573.99
4	$T_{\eta(LiAl)}$—nucleation of η(LiAl) phase	–	554.97	539.16	–
5	T_{SOL}—solidus temperature	553.48	536.61	522.36	518.07

(–) reaction not observed

structure (reaction registered for Mg–12Li–1.5Al + 0.2 TiB and Mg–12Li–1.5Al + 0.2Sr alloys).

Conclusions

The crystallisation sequence of Mg–Li–Al alloys has been investigated in detail by using thermal-derivative analysis and microstructural observations. The results are summarised as follows:

1. The TiB and Sr grain modifiers improve the microstructure of the resulting alloy. The application of TiB and Sr refines the grain of α-Mg, the grain size becomes smaller and the morphology of the grains is a small spherical crystal.
2. Microstructure and XRD analysis show that the application of TiB and Sr does not change structural and phase composition of analysed ultralight alloys. The as-cast Mg–4.5Li–1.5Al alloy comprises α(Mg) phase and Mg–12Li–1.5Al is composed of β(Li) phase.
3. The solidification time of analysed alloys is increased by increasing the Li content.
4. The most potent effect on hardness was observed when TiB as a grain refinement was added. The hardness of Mg–4.5Li–1.5Al rises from 34 to 40 HRF, and hardness of Mg–12Li–1.5Al rises from 70 to 79 HRF.
5. Based on the results of TDA, a crystallisation process of Mg–Li–Al alloys was proposed. Addition of grain refinements to the alloy with 4.5 mass% of Li causes a decrease in nucleation, slightly Mg growth temperature and strongly solidus temperature, as well as increase in the crystallisation range of the alloy from 82 °C to over 110 °C. Analysis of thermal results of the alloy containing 12 mass% of lithium shows that addition TiB and Sr causes reduction in nucleation temperature, Li growth temperature and strongly solidus temperature. Thermal analysis of the alloys containing 12 mass% of Li revealed that the crystallisation range

of the alloy increases from approx. 30 °C to over 60 °C.
6. Application of thermal-derivative analysis to characterise a solidification pathway of Mg–Li–Al alloys has large potential in the field of heat treatment and casting processes such as semisolid metal casting.

References

1. Jafari H, Khalilnezhad M, Farahany S. Computer-aided cooling curve thermal analysis and microstructural evolution of Mg–5Zn–xY cast alloys. J Therm Anal Calorim. 2017;130(3):1429–37.
2. Sroka M, Zieliński A, Hernas A, Kania Z, Rozmus R, Tański T, Śliwa A. The effect of long-term impact of elevated temperature on changes in the microstructure of Inconel 740H alloy. Metalurgija. 2017;56(3–4):333–6.
3. You S, Huang Y, Kainer KU, Hort N. Recent research and developments on wrought magnesium alloys. J Magnes Alloys. 2017;5(3):239–53.
4. Pan F, Yang M, Chen X. A review on casting magnesium alloys: modification of commercial alloys and development of new alloys. J Mater Sci Technol. 2016;32(12):1211–21.
5. Joosta WJ, Krajewski PE. Towards magnesium alloys for high-volume automotive applications. Scripta Mater. 2017;128:107–12.
6. Krupinski M, Krupinska B, Labisz K, Rdzawski Z, Tanski T. Effect of chemical composition modification on structure and properties of the cast Zn–Al–Cu alloys. P I Mech Eng L-J Mat. 2016;230(3):805–12.
7. Risueño E, Gil A, Rodríguez-Aseguinolaza J, Gil A, Tello M, Faik A, D'Aguanno B. Thermal cycling testing of Zn–Mg–Al eutectic metal alloys as potential high-temperature phase change

materials for latent heat storage. J Therm Anal Calorim. 2017;129(2):885–94.

8. Luo AA. Magnesium casting technology for structural applications. J Magn Alloys. 2013;1(1):2–22.

9. Regenera D, Tkachenko V. Strength characteristics of Mg–Li alloys. Strength Mater. 2009;41:294–302.

10. Król M, Staszuk M, Mikuszewski T, Kuc D. Refinement effect of RE in light weight Mg–Li–Al alloys. J Therm Anal Calorim. 2018;13(1):333–41. https://doi.org/10.1007/s10973-018-7290-z.

11. Król M, Tański T, Matula G, Snopiński P, Tomiczek AE. Analysis of crystallisation process of cast magnesium alloys based on thermal derivative analysis. Arch Metall Mater. 2015;60(4):2993–9. https://doi.org/10.1515/amm-2015-0478.

12. Krupińska B, Rdzawski Z. Effect of Re addition of solidification and heat treatment on the Cu-Ni-Si alloy structure. J Therm Anal Calorim. 2018;134(1):173–9.

13. Zieliński A, Sroka M, Hernas A, Kremzer M. The effect of long-term impact of elevated temperature on changes in microstructure and mechanical properties of HR3C steel. Arch Metall Mater. 2016;61(2A):761–6. https://doi.org/10.1515/amm-2016-0129.

14. Yavari F, Shabestari SG. Effect of cooling rate and Al content on solidification characteristics of AZ magnesium alloys using cooling curve thermal analysis. J Therm Anal Calorim. 2017;129:655–62. https://doi.org/10.1007/s10973-017-6240-5.

15. Nayeb-Hashemi AA, Clark JB, Pelton AD. Bull Alloy Phase Diagr. 1984;5(4):365–74.

16. Goel NC, Cahoon JR. Bull Alloy Phase Diagr. 1990;11:528. https://doi.org/10.1007/BF02841712.

17. A.I.H. Committee (1992) ASM Handbook, vol 3: Alloy Phase Diagrams, tenth edn., The Materials Information Company.

18. Król M. Effect of grain refinements on the microstructure and thermal behaviour of Mg–Li–Al alloy. J Therm Anal Calorim. 2018;133(1):237–46. https://doi.org/10.1007/s10973-018-7223-x.